

Supporting Information to
"Structural Investigation of Aluminium Doped ZnO
Nanoparticles by Solid State Spectroscopy"

Yamini S. Avadhut ^[a], *Johannes Weber* ^[a], *Elin Hammarberg* ^[b], *Claus Feldmann* ^[b],

Jörn Schmedt auf der Günne ^[a]

^[a] Ludwig-Maximilians-Universität München, Department Chemie,

Butenandtstraße 5-13 (D), D-81377 München, Germany

^[b] Institut für Anorganische Chemie, Karlsruhe Institute of Technology (KIT),

Engesserstraße 15, D-76131 Karlsruhe, Germany.

Table of Contents

1. SEM images of various AZO samples.....	3
2. ^1H MAS NMR.....	4
3. ^{13}C CPMAS NMR.....	5
4. 2D $^1\text{H}\{^{13}\text{C}\}$ Correlation NMR.....	5
5. $^{27}\text{Al}\{^1\text{H}\}$ 2D HETCOR.....	6
6. Computational Details.....	7
6.1. Structure optimizations.....	7
6.1.1. The Al_{Zn} defect site.....	10
6.1.2. The $\text{Al}_{i,\text{Td}}$ interstitial site.....	15
6.1.3. Optimization of the $\text{Al}_{i,\text{Oh}}$ interstitial site.....	16
6.1.4. Optimization of the $[\text{Al}_2\text{V}_{\text{Zn}}]$ defect site	17
6.2. Calculation of ^{27}Al NMR parameters by EEIM.....	20
7. References.....	25

1. SEM images of various AZO samples

Scanning electron microscopy (SEM) investigations on as-prepared AZO samples (1.0, 1.8 and 4.9 mol-%) were carried out with a Zeiss Supra 40 VP microscope (see Figure S1). Diluted suspensions in DEG were deposited on silicon wafers, evaporated and sputtered with Pt. The acceleration voltage and the working distance were 10 kV and 3 mm, respectively. Statistical evaluation of particle size and size distribution was performed based on the software package Scandium 5.0 from Soft Imaging Systems.

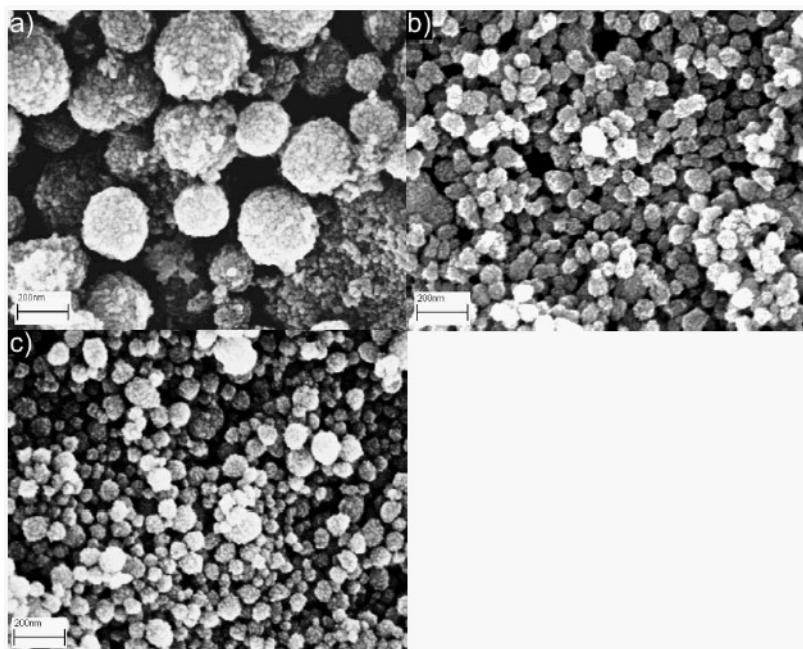


Figure S1: SEM images of AZO-ap samples with Al:Zn molar ratios of a) 1 %, b) 1.8 % and c) 4.9 %; powders redispersed in ethanol.

2. ^1H MAS NMR

Figure S2 shows comparison of quantitative ^1H MAS NMR spectra of aluminium doped zinc oxide (1.8 mol-%) with different heat treatment namely as-prepared AZO (a), oxidized at 400 °C (b), reduced with forming gas (c), and heated at 800 °C (d), respectively. It is observed that, against the common perception, the DEG/organic components have not fully vanished after heat treatment at 400 °C. Observable are peaks stemming from acetate (CH_3 -function ~ 1.2 ppm) and DEG (CH_2 -functions: 3.59 ppm and 3.74 ppm, OH broad peak ~ 4.5 ppm)

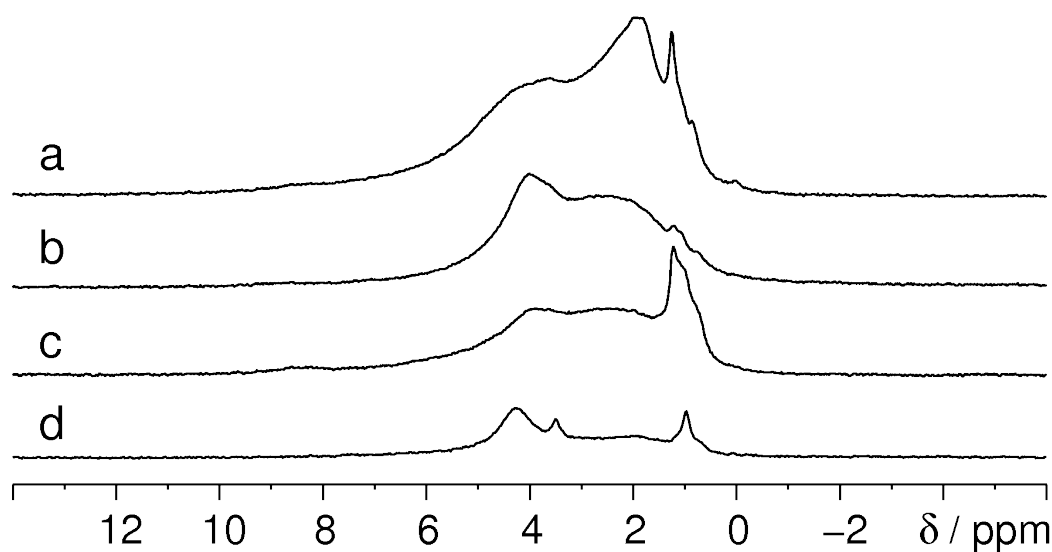


Figure S2: Quantitative ^1H MAS NMR spectra of aluminium doped zinc oxide (AZO-ap, 1.8 mol-%): (a) as-prepared, (b) heated at 400 °C, (c) reduced with forming gas, and (d) heated at 800 °C with direct excitation at a sample spinning frequency of 50 kHz using a recycle delay of 8 s; approximately the same amount of sample was packed into the rotors and similar experimental conditions were applied.

3. ^{13}C CPMAS NMR

$^{13}\text{C}\{^1\text{H}\}$ CPMAS NMR spectrum of as-prepared aluminium doped zinc oxide (1.8 mol-%) is shown in Figure S3 which is discussed in details in the main article. The peaks at 180.2 ppm and 20.9 ppm belong to acetic acid. The peaks at 71.8 and 61.4 ppm are assigned to CH_2 function of DEG.

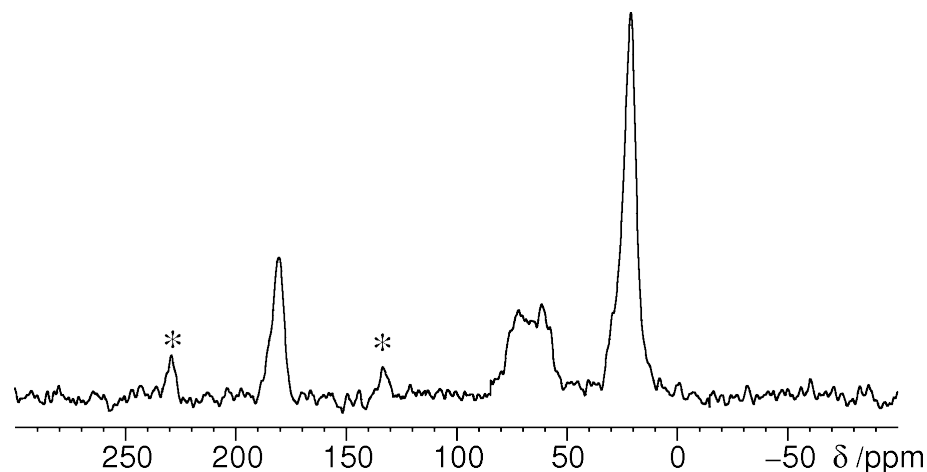


Figure S3: $^{13}\text{C}\{^1\text{H}\}$ CPMAS NMR spectrum of aluminium doped zinc oxide, (AZO-ap, 1.8 mol-%) recorded with a 1 ms contact time, recycle delay of 3 s, at a field of 11.74 T and a sample spinning frequency of 6 kHz; spinning sidebands are marked by asterisk.

4. 2D $^1\text{H}\{^{13}\text{C}\}$ Correlation NMR

Due to limited resolution of ^1H MAS NMR (Figure S2) a peak assignment requires a two dimensional $^1\text{H}\{^{13}\text{C}\}$ correlation method. The correlation is achieved by using inverse detection heteronuclear correlation spectroscopy.¹ In this experiment, the ^{13}C dimension is indirectly observed by detecting on ^1H nuclei. Figure S4 shows the inversely detected 2D $^1\text{H}\{^{13}\text{C}\}$ heteronuclear correlation spectrum of as-prepared AZO (1 mol-%). Figure S4 shows a correlation peak between methyl ^1H (1.2 ppm) and methyl ^{13}C (20.9 ppm) of acetate, which reflects the proximity of the methyl ^{13}C and methyl ^1H groups. This correlation peak confirms the presence of acetate in as-prepared aluminium doped zinc oxide nanoparticles.

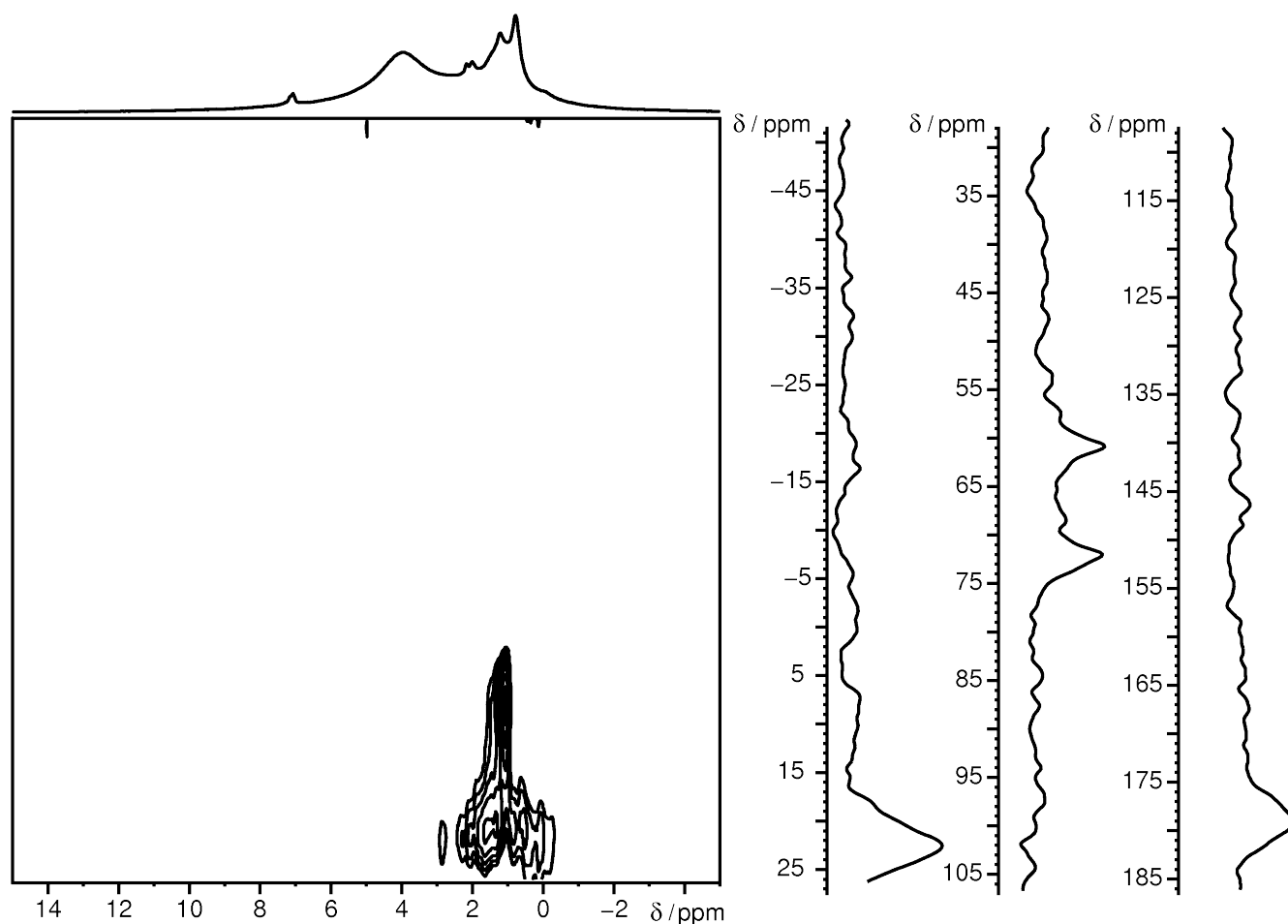


Figure S4: A 2D $^1\text{H}\{^{13}\text{C}\}$ correlation spectrum obtained with inverse detection of aluminum doped zinc oxide, (AZO-ap, 1 mol-%), recorded under MAS at 10 kHz, with 3 ms contact time, recycle delay of 2 s, at a magnetic field of 11.74 T. The projections were taken from separate 1D ^1H MAS and $^{13}\text{C}\{^1\text{H}\}$ CP-MAS experiments.

5. $^{27}\text{Al}\{^1\text{H}\}$ 2D HETCOR

Figure S5 shows the 2D $^{27}\text{Al}\{^1\text{H}\}$ PRESTO-III spectra of AZO-ox-400 (1.8 mol %) and AZO-red (1.8 mol %). Both spectra show site connectivities between the components $\text{Al}_\text{B}^{(\text{IV})}$, Al^V , and $\text{Al}^{(\text{VI})}$ and the ^1H NMR signals from DEG and acetic acid/acetate. Hence, the 2D $^{27}\text{Al}\{^1\text{H}\}$ PRESTO-III spectra reconfirm the presence of DEG and acetic acid/acetate even after heat treatment at 400 °C and reductive treatment.

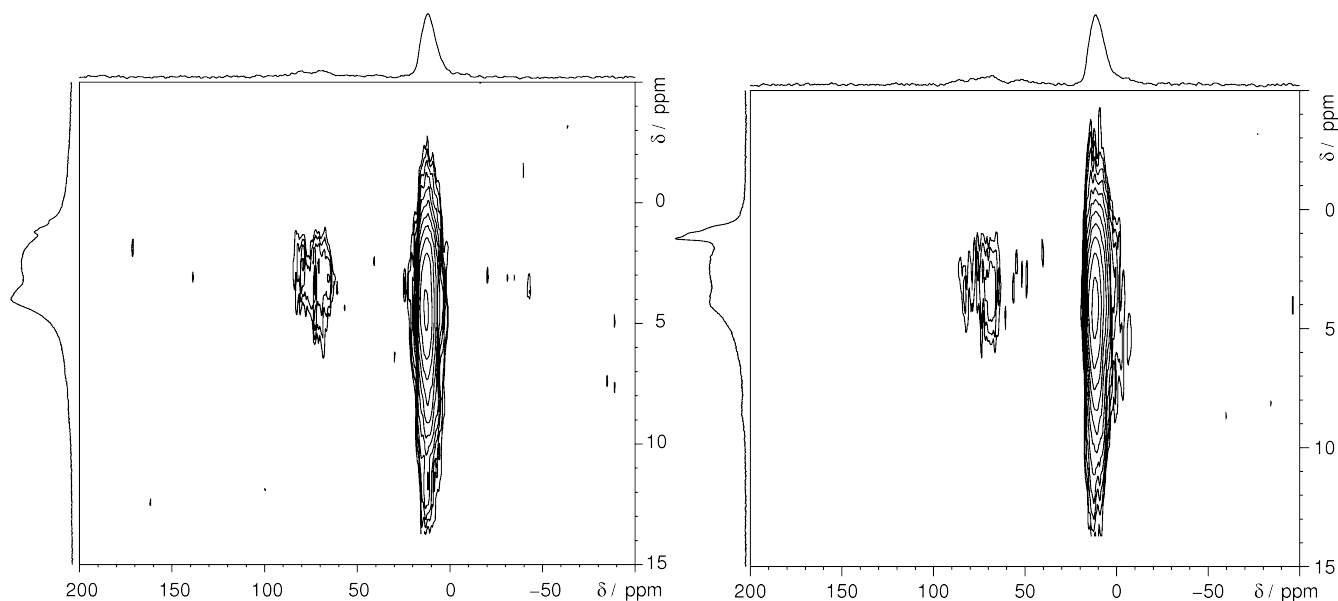


Figure S5: $^{27}\text{Al}\{^1\text{H}\}$ 2D HETCOR spectra of aluminum doped zinc oxide nanoparticles. *left:* AZO-ox-400 (1.8 mol %), *right:* AZO-red (1.8 mol %). Spectra were acquired at a field of 11.74 T and a spinning frequency of 10 kHz using a ^1H - ^{27}Al PRESTO-III pulse sequence (detailed explanation in the main article); the ^1H projection was taken from separate 1D single-pulse excitation experiment; additionally, a sum projection of the 2D PRESTO-III projection is shown for the ^{27}Al dimension.

6. Computational Details

This section provides further details on the performed computations, which had to be removed from the main text for brevity. Part of it is redundant with the main text in order to enhance readability.

6.1. Structure optimizations

Calculations were performed by a supercell approach under periodic boundary conditions with the VASP program, version 4.6.28, at PBE/PAW level as described in the main text. Here, we mention further details. The tetrahedron method with Blöchl's corrections² was used for Brillouin-zone integration. Electronic wave functions were considered as converged if the energy change in subsequent SCF cycles was below 10^{-8} eV. The Quasi-Newton method was used to derive structural relaxation steps.

Starting from the default, *wurtzite*-like ZnO structure of Heller *et al.*³ (ICSD 76641) that has space

group symmetry $P6_3mc$ (No 186), cell parameters of $a = b = 3.2495 \text{ \AA}$, $c = 5.2069 \text{ \AA}$, $\alpha = \beta = 90^\circ$, $\gamma = 120^\circ$ and four atoms per unit cell, the supercell was chosen as a $3 \times 3 \times 2$ expansion of the ZnO cell, thus containing 36 Zn-atoms and 36 O-atoms. Subsequently, one of the point defects was built in and various partial structure optimizations were performed (Al-atoms only, Al plus 1st coordination sphere, Al plus 1st and 2nd coordination sphere) as well as full optimizations of all fractional coordinates. Supercell parameters were kept constant at $a = b = 9.7485 \text{ \AA}$, $c = 10.4138 \text{ \AA}$ in all calculations. The energy dependence on various automatically generated k -point grids according to the *Monkhorst-Pack* scheme⁴ was tested. Finally, a Γ -centered k -point grid with four points in each direction ($4 \times 4 \times 4$) was used, which turned out to be sufficiently dense to yield absolute energy convergence of $\text{AlZn}_{35}\text{O}_{36}$ to 0.003 eV (= 4 kJ/mol). Symmetries of the doped supercells were initially maintained at $P3m1$ (No. 156) for Al_{Zn} , $\text{Al}_{i,\text{Td}}$, $\text{Al}_{i,\text{Oh}}$ during the optimizations, but were released subsequently to $P1$ (No 1) by slight displacements of the dopant in order to check for Jahn-Teller-distortions⁵ of lower energy. The three variants of the $[\text{Al}_2\text{V}_{\text{Zn}}]$ -defect and the defect combinations $[\text{Al}_{i,\text{Td}}\text{V}_{\text{Zn}}]$, $[\text{Al}_{i,\text{Oh}}\text{V}_{\text{Zn}}]$ were treated in space group $P1$.

Also, the number of valence electrons (e_{val}^-) was varied in order to investigate its influence on the defect structure. By default each elemental Zn has 12 e_{val}^- , each elemental O 6 e_{val}^- and each elemental Al 3 e_{val}^- within the calculation scheme, resulting in 639 e_{val}^- for $\text{AlZn}_{35}\text{O}_{36}$, i.e. the electroneutral cell is an open-shell system with one unpaired electron. However, if we consider the substitution as an exchange of Zn^{2+} by Al^{3+} the number of electrons is reduced to 638 e_{val}^- (this could be termed as p -type doping). On the other hand, if we want to consider a more n -doped system with a closed-shell configuration, we need 640 e_{val}^- , which would correspond to an exchange of Zn^{2+} with Al^+ , formally. For all three types of doping, spin-polarization free calculations have been performed on Al_{Zn} . By default, deviations from charge neutrality within a unit cell are compensated in VASP by defining a homogeneously distributed counter charge (*jellium background*). No compensation mechanism for higher electrical moments is used. Table S1 gives an overview of the performed calculations as well as their energies in col. 6. The structural effects are discussed in the subsequent paragraphs, CIF files for each optimized structure are delivered with this document. CIF file names are chosen according to the calculation number in Table S1.

Table S1: Total energies of 3x3x2 supercells with various defects as calculated at PBE/PAW level in VASP (col. 6). Col. 1 holds the calculation number, col. 2 the defect type, col. 3 the relaxed part of the supercell, col. 4 the assumed cell symmetry, col. 5 the number of valence electrons per unit cell, col. 7 the number of k-points in the directions of the reciprocal space and col. 8 the energy cutoff of the plane wave expansion; CIF files containing the listed defect structures can be found in the supporting information and are named according to the "calc. no.".

Calc. no.	defect	Relaxed part	Cell Symmetry	# e^-	$E_{\text{total}} / \text{eV}$	# k -points	$E_{\text{cut}} / \text{eV}$
0	$\text{Al}_{\text{Zn}}^{(0)}$	none	$P3m1$	639	-331.25552407	4x4x4	500
1	$\text{Al}_{\text{Zn}}^{(1+)}$	Al	$P3m1$	638	-334.16316930	4x4x4	500
2	$\text{Al}_{\text{Zn}}^{(0)}$	Al	$P3m1$	639	-331.26777987	4x4x4	500
3	$\text{Al}_{\text{Zn}}^{(1-)}$	Al	$P3m1$	640	-327.76446600	4x4x4	500
4	$\text{Al}_{\text{Zn}}^{(1+)}$	AlO_4	$P3m1$	638	-335.37212468	4x4x4	500
5	$\text{Al}_{\text{Zn}}^{(0)}$	AlO_4	$P3m1$	639	-332.45491438	4x4x4	500
6	$\text{Al}_{\text{Zn}}^{(1-)}$	AlO_4	$P3m1$	640	-328.93294249	4x4x4	500
7	$\text{Al}_{\text{Zn}}^{(1+)}$	$\text{AlO}_4\text{Zn}_{12}$	$P3m1$	638	-335.40376669	4x4x4	500
8	$\text{Al}_{\text{Zn}}^{(0)}$	$\text{AlO}_4\text{Zn}_{12}$	$P3m1$	639	-332.48360601	4x4x4	500
9	$\text{Al}_{\text{Zn}}^{(1-)}$	$\text{AlO}_4\text{Zn}_{12}$	$P3m1$	640	-328.95911095	4x4x4	500
10	$\text{Al}_{\text{Zn}}^{(1+)}$	full	$P3m1$	638	-335.54170813	4x4x4	500
11	$\text{Al}_{\text{Zn}}^{(0)}$	full	$P3m1$	639	-332.61465545	4x4x4	500
12	$\text{Al}_{\text{Zn}}^{(1-)}$	full	$P3m1$	640	-329.08311640	4x4x4	500
13	$\text{Al}_{\text{Zn}}^{(1+)}$	Al	$P1$	638	-334.16317084	4x4x4	500
14	$\text{Al}_{\text{Zn}}^{(0)}$	Al	$P1$	639	-331.26778127	4x4x4	500
15	$\text{Al}_{\text{Zn}}^{(1-)}$	Al	$P1$	640	-327.76446759	4x4x4	500
16	$\text{Al}_{\text{Zn}}^{(1+)}$	AlO_4	$P1$	638	-335.37217452	4x4x4	500
17	$\text{Al}_{\text{Zn}}^{(0)}$	AlO_4	$P1$	639	-332.45496646	4x4x4	500
18	$\text{Al}_{\text{Zn}}^{(1-)}$	AlO_4	$P1$	640	-328.93299428	4x4x4	500
19	$\text{Al}_{\text{Zn}}^{(1+)}$	$\text{AlO}_4\text{Zn}_{12}$	$P1$	638	-335.40386025	4x4x4	500
20	$\text{Al}_{\text{Zn}}^{(0)}$	$\text{AlO}_4\text{Zn}_{12}$	$P1$	639	-332.48370112	4x4x4	500
21	$\text{Al}_{\text{Zn}}^{(1-)}$	$\text{AlO}_4\text{Zn}_{12}$	$P1$	640	-328.95921854	4x4x4	500
22	$\text{Al}_{\text{Zn}}^{(1+)}$	full	$P1$	638	-335.54193373	4x4x4	500
23	$\text{Al}_{\text{Zn}}^{(0)}$	full	$P1$	639	-332.61488943	4x4x4	500
24	$\text{Al}_{\text{Zn}}^{(1-)}$	full	$P1$	640	-329.08332917	4x4x4	500
25	$\text{Al}_{i,\text{Td}}^{(0)}$	initial (see text)	$P3m1$	651	-308.20341473	4x4x4	500
26	$\text{Al}_{i,\text{Td}}^{(0)}$	Al	$P3m1$	651	-318.39535382	4x4x4	500
27	$\text{Al}_{i,\text{Td}}^{(0)}$	$\text{Al}_{i,\text{Td}}\text{O}_4\text{Zn}_4$	$P3m1$	651	-324.80934174	4x4x4	500
28	$\text{Al}_{i,\text{Oh}}^{(0)}$	initial (see text)	$P3m1$	651	-322.84030193	4x4x4	500
29	$\text{Al}_{i,\text{Oh}}^{(0)}$	Al	$P3m1$	651	-324.50176712	4x4x4	500

Calc. no.	defect	Relaxed part	Cell Symmetry	# e^-	$E_{\text{total}} / \text{eV}$	# k -points	$E_{\text{cut}} / \text{eV}$
30	$\text{Al}_{\text{i,Oh}}^{(0)}$	$\text{Al}_{\text{i,Oh}}\text{O}_4\text{Zn}_4$	$P3m1$	651	-326.99241765	4x4x4	500
31	none(ZnO)	3x3x2 supercell	$P6_3mc$	648	-326.76976112	4x4x4	500
32	full, ZnO	3x3x2 supercell	$P6_3mc$	648	-326.89813177	4x4x4	500
33	$\text{Al}_{\text{i,Oh}}V_{\text{Zn}}$	Non opt	Pm	639	-322.80023658	4x4x4	500
34	$\text{Al}_{\text{i,Oh}}V_{\text{Zn}}$	Al-opt	Pm	639	-331.26778106	4x4x4	500
35	$\text{Al}_{\text{i,Td}}V_{\text{Zn}}$	Non opt	$P3m1$	639	-327.25049921	4x4x4	500
36	$\text{Al}_{\text{i,Td}}V_{\text{Zn}}$	Al-opt	$P3m1$	639	-331.26777979	4x4x4	500
37	$\text{Al}_2V_{\text{Zn}} i)$	Non opt	$P1$	618	-332.14337857	4x4x4	500
38	$\text{Al}_2V_{\text{Zn}} i)$	Al-opt	$P1$	618	-332.20270127	4x4x4	500
39	$\text{Al}_2V_{\text{Zn}} i)$	1 st sphere opt	$P1$	618	-335.00718144	4x4x4	500
40	$\text{Al}_2V_{\text{Zn}} ii)$	Non opt	$P1$	618	-332.11422101	4x4x4	500
41	$\text{Al}_2V_{\text{Zn}} ii)$	Al-opt	$P1$	618	-332.18848019	4x4x4	500
42	$\text{Al}_2V_{\text{Zn}} ii)$	1 st sphere opt	$P1$	618	-334.91637520	4x4x4	500
43	$\text{Al}_2V_{\text{Zn}} iii)$	Non opt	$P1$	618	-332.00894371	4x4x4	500
44	$\text{Al}_2V_{\text{Zn}} iii)$	Al-opt	$P1$	618	-332.15063989	4x4x4	500
45	$\text{Al}_2V_{\text{Zn}} iii)$	1 st sphere opt	$P1$	618	-334.72814086	4x4x4	500

6.1.1. The Al_{Zn} defect site

The Al_{Zn} site is simulated by replacing one Zn atom by Al in the 3x3x2 supercell of ZnO. On PBE/PAW level the total energy per supercell amounts to -331.256 eV (calc. 0).

Optimization of the Al_{Zn} position. If only the Al_{Zn} position is optimized in space group symmetry $P3m1$ (No 156), an energetic stabilization of -0.012 eV(=-1.2 kJ/mol) is observed (calc. 2, 639 e^-) in conjunction with a displacement in the range of 0.01 Å along the c -axis, that reduces the bond length differences between Al and its axial or non-axial O-atoms (see Table S2). The result is independent of the number of electrons (calculations have been performed with 638 e^- , 639 e^- , and 640 e^-). Allowing the same optimization in $P1$ (No 1) results in practically the same structures; the displacement in the range of 0.001 Å relative to the symmetry-restricted Al_{Zn} optimization and an energy stabilization of 1.5 J/mol has more likely its origin in numerical issues rather than a true Jahn-Teller distortion.

Table S2: Comparison of structural parameters from optimizations of the Al_{Zn} site, only. Al_{unrelaxed} denotes the unrelaxed Al position.

Calculation	$d(\text{Al}-\text{Al}_{\text{unrelaxed}})/\text{Å}$	$d(\text{Al}-\text{O13}_{\text{ax}})/\text{Å}$	$d(\text{Al}-\text{O1})/\text{Å}$	$d(\text{Al}-\text{O10})/\text{Å}$	$d(\text{Al}-\text{O11})/\text{Å}$
0. unrelaxed	0,000	1,953	1,986	1,986	1,986
1.(638 e^- , $P3m1$)	0,010	1,963	1,982	1,982	1,982
2.(639 e^- , $P3m1$)	0,011	1,963	1,982	1,982	1,982
3.(640 e^- , $P3m1$)	0,010	1,963	1,982	1,982	1,982
13.(638 e^- , $P1$)	0,010	1,963	1,983	1,982	1,982
14.(639 e^- , $P1$)	0,010	1,963	1,983	1,982	1,982
15.(640 e^- , $P1$)	0,011	1,963	1,983	1,982	1,982

Optimization of Al_{Zn}O₄. Optimization of the Al position together with its first coordination sphere, i.e. the four nearest neighbors O_i , $i=\{13, 1, 10, 11\}$, results in a significant stabilization of 1.199 eV (= -115.7 kJ/mol, calc. 5, 639 e^-) as compared to the unrelaxed structure. Selected structural parameters and comparisons to the unrelaxed structure are shown in Table S3. The Al position is hardly altered. The Al- O_i distances are significantly shortened by 0.16 Å (O13) or 0.19 Å (O1,O10,O13). A shortening of the Al- O_i distances is expected because of the smaller ionic radius of Al as compared to Zn. Furthermore, the difference $|d(\text{Al}-\text{O13})-d(\text{Al}-\text{O1}/10/13)|$ between the Al-O13 bond length along the c -axis and the other three Al-O bonds is significantly decreased from 0.033 Å in the unrelaxed structure to ≤ 0.005 Å in the VASP optimized one. Thus, the AlO₄ unit comes significantly closer to an ideal tetrahedron. The distances of O_i to their neighboring Zn atoms is increased by 0.09 Å to 2.044 Å (O13) and by {0.08, 0.06} Å to {2.035,2.051} Å for O1, O10, O11 (these atoms have two different O-Zn distances). Variation of the defect charge in the row of calcs. 4. to 6. (with 638 to 640 e^-) leads to very small, yet systematic, changes of atomic positions in the range ≤ 0.005 Å. The averaged Al-O distance decreases slightly with increasing number of e^- .

The same optimizations in space group $P1$ (No 1) (calcs. 16-18) result in practically the same structures; with displacements in the range of 0.002 Å and an energy stabilization of 5 J/mol, which is no clear indication for a Jahn-Teller distortion.

Table S3: Comparison of structural parameters from optimizations of $\text{Al}_{\text{Zn}}\text{O}_4$.

Calculation	$d(X-X_{\text{unrelaxed}})/\text{\AA}$					$d(\text{Al}-X)/\text{\AA}$			
	$X=\text{Al}$	O13	O1	O10	O11	O13 _{ax}	O1	O10	O11
0. unrelaxed	0,000	0,000	0,000	0,000	0,000	1,953	1,986	1,986	1,986
4.(638 e^- , $P3m1$)	0,002	0,160	0,187	0,187	0,187	1,794	1,799	1,799	1,799
5.(639 e^- , $P3m1$)	0,001	0,160	0,189	0,189	0,189	1,794	1,797	1,797	1,797
6.(640 e^- , $P3m1$)	0,000	0,160	0,192	0,192	0,192	1,793	1,795	1,795	1,795
16.(638 e^- , $P1$)	0,003	0,160	0,189	0,186	0,186	1,794	1,799	1,799	1,799
17.(639 e^- , $P1$)	0,002	0,160	0,191	0,188	0,188	1,794	1,797	1,797	1,797
18.(640 e^- , $P1$)	0,002	0,160	0,193	0,190	0,190	1,793	1,795	1,795	1,795

Optimization of $\text{Al}_{\text{Zn}}\text{O}_4\text{Zn}_{12}$. The shorthand notation “ $\text{Al}_{\text{Zn}}\text{O}_4\text{Zn}_{12}$ ” indicates an optimization of the Al position together with its first (O_i , see above) and second coordination sphere (Zn_j , $j=\{1, 2, 5, 9, 10, 11, 17, 18, 22, 24, 27, 28\}$). It results in an energetic stabilization of -118.5 kJ/mol (calc. 8, 639 e^-) compared to the unrelaxed structure, which is a gain of only 2.8 kJ/mol as compared to the optimization of $\text{Al}_{\text{Zn}}\text{O}_4$. Selected structural parameters of the first coordination sphere and comparisons to the unrelaxed structure are shown in Table S4. The difference $|d(\text{Al}-\text{O13})-d(\text{Al}-\text{O1})|$ between the Al-O13 bond length along the c -axis and the other three Al-O bonds is $<0.003 \text{ \AA}$, i.e. further decreased as compared to $\text{Al}_{\text{Zn}}\text{O}_4$. Position changes in the second coordination sphere are about 0.018 \AA for most Zn atoms, which is one order of magnitude smaller than those in the first coordination sphere. A bigger change of 0.042 \AA is obtained for Zn28 (and the symmetry equivalent Zn11, Zn18), however. As in $\text{Al}_{\text{Zn}}\text{O}_4$, a very weak dependence on the defect charge is predicted, with slightly decreasing average Al-O distances going along with an increasing number of e^- .

The $\text{Al}_{\text{Zn}}\text{O}_4\text{Zn}_{12}$ optimizations in space group $P1$ (No 1) yield very similar structures; with displacements $\leq 0.004 \text{ \AA}$ and energy stabilizations of about 10 J/mol, which indicates that a very small Jahn-Teller distortion might be present. It is unlikely however, that this leads to a statically distorted structure at room temperature, because the different local minima on the potential energy surface should be thermally accessible.

Table S4: Comparison of structural parameters from optimizations of $\text{Al}_{\text{Zn}}\text{O}_4\text{Zn}_{12}$.

Calculation	$d(X-X_{\text{unrelaxed}})/\text{Å}$								$d(\text{Al}-X)/\text{Å}$			
	X=Al	O13	O1	O10	O11	Zn2	Zn9	Zn28	O13 _{ax}	O1	O10	O11
0. unrelaxed	0,000	0,000	0,000	0,000	0,000	0,000	0,000	0,000	1,953	1,986	1,986	1,986
7.(638 e^-)	0,023	0,175	0,175	0,175	0,175	0,015	0,019	0,042	1,800	1,803	1,803	1,803
8.(639 e^-)	0,021	0,175	0,179	0,179	0,179	0,016	0,019	0,037	1,799	1,801	1,801	1,801
9.(640 e^-)	0,018	0,174	0,183	0,183	0,183	0,018	0,020	0,033	1,797	1,797	1,797	1,797
19.(638 e^- , P1)	0,023	0,175	0,178	0,174	0,174	0,015	0,019	0,041	1,800	1,803	1,803	1,803
20.(639 e^- , P1)	0,021	0,175	0,181	0,177	0,177	0,016	0,019	0,037	1,798	1,800	1,800	1,801
21.(640 e^- , P1)	0,018	0,173	0,187	0,181	0,181	0,018	0,020	0,032	1,797	1,797	1,797	1,797

Full optimization. We denote the optimization of all 72 atomic sites in the $3 \times 3 \times 2$ supercell as *full optimization* of $\text{Al}_{\text{Zn}}\text{O}_{36}\text{Zn}_{35}$. This optimization results in an energetic stabilization of -129.9 kJ/mol (calc. 11; 639 e^-) compared to the unrelaxed structure, i.e. further stabilization of -11.4 kJ/mol in comparison to $\text{Al}_{\text{Zn}}\text{O}_4\text{Zn}_{12}$. At first view, this seems larger than expected, because stabilization energies in the row $\text{Al}_{\text{Zn}} \rightarrow \text{Al}_{\text{Zn}}\text{O}_4 \rightarrow \text{Al}_{\text{Zn}}\text{O}_4\text{Zn}_{12}$ decrease rapidly, which is in line with the picture of a local defect that induces the most significant structural changes of the bulk material in its vicinity. However, one has to consider, that in the full optimization not only the stress from the defective site is relaxed, but also the structural difference between the experimental and the calculated equilibrium structure of the ZnO-bulk, which amounts to -12.3 kJ/mol for the $3 \times 3 \times 2$ supercell (calcs. 31+32)[†]. This indicates that changes outside the second coordination sphere of the dopant are probably below 1 kJ/mol. For an accurate measure one would require a larger supercell.

Selected structural parameters of the first coordination sphere and comparisons to the unrelaxed structure are shown in Table S5. Compared to the previous calculations the difference $|d(\text{Al}-\text{O13})-d(\text{Al}-\text{O1})|$ between the Al-O13 bond length along the c -axis and the other three Al-O bonds is further decreased to ≤ 0.002 Å. Position changes in the second coordination sphere are ≤ 0.02 Å for all Zn atoms, which is one order of magnitude smaller than those in the first coordination sphere. As in the previous calculations, a weak decrease of the Al-O distances is obtained, if the number of e^- in the system is increased.

[†] Notably, significant changes in atomic distances are obtained for bulk ZnO when it is optimized at PBE/PAW level: $d(\text{Zn}, \text{O13}_{\text{ax}})$ changes from 1.953 Å to 1.983 Å and $d(\text{Zn}, \text{O1}_{\text{eq}})$ changes from 1.986 Å to 1.976 Å, i.e. $d(\text{Zn}, \text{O13}_{\text{ax}}) > d(\text{Zn}, \text{O1}_{\text{eq}})$ after optimization. This result was checked to be independent of the choice of k -points and the σ (smearing) parameter.

Conduction of the full optimizations in space group $P1$ (No 1) lead to very similar structures; with displacements $\leq 0.004 \text{ \AA}$ and energy stabilizations $< 23 \text{ J/mol}$. which indicates that even if a small Jahn-Teller effect was present, the effective local symmetry for the ^{27}Al NMR experiment would still have a C_3 symmetry axis, because the thermal energy at room temperature is higher than the energetic stabilization by a factor of about 100.

Table S5: Comparison of structural parameters from full optimizations of $\text{Al}_{\text{Zn}}\text{O}_{36}\text{Zn}_{35}$.

Calculation	$d(X-X_{\text{unrelaxed}})/\text{\AA}$									$d(\text{Al-X})/\text{\AA}$			
	X=Al	O13	O1	O10	O11	Zn2	Zn9	Zn28	O13 _{ax}	O1	O10	O11	
0. unrelaxed	0,000	0,000	0,000	0,000	0,000	0,000	0,000	0,000	1,953	1,986	1,986	1,986	
10.(638 e^-)	0,004	0,160	0,187	0,187	0,187	0,019	0,019	0,010	1,797	1,799	1,799	1,799	
11.(639 e^-)	0,004	0,161	0,189	0,189	0,189	0,019	0,019	0,008	1,796	1,797	1,797	1,797	
12.(640 e^-)	0,002	0,161	0,193	0,193	0,193	0,019	0,019	0,005	1,794	1,794	1,794	1,794	
22.(638 e^- , $P1$)	0,006	0,160	0,190	0,185	0,185	0,020	0,018	0,011	1,797	1,799	1,799	1,799	
23.(639 e^- , $P1$)	0,005	0,161	0,192	0,187	0,187	0,020	0,019	0,008	1,796	1,797	1,797	1,797	
24.(640 e^- , $P1$)	0,005	0,161	0,197	0,191	0,191	0,020	0,019	0,006	1,794	1,794	1,794	1,794	

In contrast to the previous Hartree-Fock based study by Maldonado and Stashans,¹⁵ we find a local C_3 pseudo-pointgroup symmetry of the Al_{Zn} site with the rotation axis along the crystal c -axis. The significant differences might indicate a flat potential for displacements of the atoms in the AlO_4 unit. The calculated deviations from C_3 symmetry are very small in our case and may be caused by numerical inaccuracies. In any way, the EFG anisotropy η_Q is predicted to be close to 0, no matter whether the Al_{Zn} site has precise C_3 symmetry or only approximate. This is in agreement with the experimental findings. Deviations of the AlO_4 unit from T_d symmetry are small, but clearly visible in the bond angles. Moreover, the atomic sites in the outer shells adapt more and more to the wurtzite type structure, so that we expect a small but not vanishing EFG (V_{zz}). Figure S7(a) shows the local Al_{Zn} structure of calc. 20, which is representative of all calculations performed under periodic boundary conditions.

Table S6: Comparison of bond angles from all optimizations performed on Al_{Zn}.

Calculation	Bond angles $\angle(i-j-k)/\text{deg}$					
	O13-Al-O1	O13-Al-O10	O13-Al-O11	O1-Al-O10	O1-Al-O11	O10-Al-O11
0. unrelaxed	109,13	109,13	109,13	109,81	109,81	109,81
1.(638 e^- , Al)	108,85	108,85	108,85	110,09	110,09	110,09
2.(639 e^- , Al)	108,84	108,84	108,84	110,10	110,10	110,10
3.(640 e^- , Al)	108,85	108,85	108,85	110,09	110,09	110,09
4.(638 e^- , Al _{Zn} O ₄)	108,64	108,64	108,64	110,29	110,29	110,29
5.(639 e^- , Al _{Zn} O ₄)	108,63	108,63	108,63	110,30	110,30	110,30
6.(640 e^- , Al _{Zn} O ₄)	108,63	108,63	108,63	110,30	110,30	110,30
7.(638 e^- , Al _{Zn} O ₄ Zn ₁₂)	108,60	108,60	108,60	110,32	110,32	110,32
8.(639 e^- , Al _{Zn} O ₄ Zn ₁₂)	108,61	108,61	108,61	110,32	110,32	110,32
9.(640 e^- , Al _{Zn} O ₄ Zn ₁₂)	108,64	108,64	108,64	110,29	110,29	110,29
10.(638 e^- , full opt)	108,32	108,32	108,32	110,59	110,59	110,59
11.(639 e^- , full opt)	108,33	108,33	108,33	110,59	110,59	110,59
12.(640 e^- , full opt)	108,38	108,38	108,38	110,54	110,54	110,54
13.(638 e^- , Al _{Zn} , P1)	108,84	108,86	108,86	110,07	110,08	110,10
14.(639 e^- , Al _{Zn2} , P1)	108,83	108,85	108,86	110,08	110,08	110,10
15.(640 e^- , Al _{Zn} , P1)	108,82	108,86	108,85	110,08	110,07	110,11
16.(638 e^- , Al _{Zn} O ₄ , P1)	108,57	108,67	108,67	110,29	110,29	110,29
17.(639 e^- , Al _{Zn} O ₄ , P1)	108,57	108,67	108,67	110,30	110,30	110,29
18.(640 e^- , Al _{Zn} O ₄ , P1)	108,57	108,66	108,60	110,30	110,31	110,29
19.(638 e^- , Al _{Zn} O ₄ Zn ₁₂ ,P1)	108,58	108,60	108,60	110,31	110,31	110,40
20.(639 e^- , Al _{Zn} O ₄ Zn ₁₂ ,P1)	108,58	108,61	108,61	110,30	110,30	110,38
21.(640 e^- , Al _{Zn} O ₄ Zn ₁₂ ,P1)	108,59	108,67	108,67	110,25	110,25	110,36
22.(638 e^- , full opt, P1)	108,20	108,40	108,40	110,59	110,59	110,57
23.(639 e^- , full opt, P1)	108,24	108,40	108,40	110,58	110,58	110,56
24.(640 e^- , full opt, P1)	108,26	108,46	108,46	110,52	110,51	110,55

6.1.2. The Al_{*i,Td*} interstitial site

The Al_{*i,Td*} interstitial site is located on an axis parallel to the crystal *c*-axis that connects a Zn atom and its shortest distant O neighbor. Initially, the Al atom was placed at the tetrahedral void of that O-site at a distance of 1.953 Å and opposite to the Zn atom. This implied a distance of 1.986 Å to three other O-sites, so that the Al_{*i,Td*} interstitial had an approximately tetrahedral environment of nearest oxygen

neighbors, similar as the Zn site in undoped ZnO. In addition, there is a short Al-Zn contact present with a distance of 1.302 Å and three further Zn-sites at a distance of 2.283 Å. The total energy per $\text{Al}_{i,Td}\text{Zn}_{36}\text{O}_{36}$ supercell (3x3x2) amounts to -308.203 eV (calc. 25). All results shown in this section were calculated with $651e^-$, i.e. a formal doping with an uncharged $\text{Al}^0(=\text{Al}_{i,Td}^{+++} + 3 e^-)$ and assumption of space group symmetry $P3m1$ (No. 156).

Optimization of $\text{Al}_{i,Td}$. Relaxation of the $\text{Al}_{i,Td}$ -site only (calc. 26) results in an energetic stabilization of -10.192 eV(=-983.4 kJ/mol) and shows a significant displacement of 0.438 Å parallel to $-c$ which increases the short distance to the Zn site mentioned above to 1.740 Å, while the distance to the O-site is reduced to 1.514 Å.

Optimization of $\text{Al}_{i,Td}\text{O}_4\text{Zn}_4$. The relaxation of the Al position together with its 8 nearest neighbors (four O-, four Zn-sites)[†] (calc. 27) is denoted as $\text{Al}_{i,Td}\text{O}_4\text{Zn}_4$. The structure is stabilized by -16.606 eV(=-1602.2 kJ/mol) as compared to the non-relaxed structure (see Figure S7). At this Al changes its position by 0.419 Å along $-c$, the distance to the nearest (axial) O-site amounts to 1.643 Å, the distance to the other O-atoms reduces to 1.860 Å; the distance to the shortest Zn increases to 2.029 Å, the one to the other three Zn-sites mentioned above increases to 2.434 Å. A comparison of structural parameters is given in Table S7. Figure S7b shows the final structure of the $\text{Al}_{i,Td}$ defect obtained by calc. 27.

Table S7: Comparison of structural parameters from different optimizations of $\text{Al}_{i,Td}$ in a 3x3x2 supercell.

Calculation	$d(X-X_{\text{unrelaxed}})/\text{Å}$					$d(\text{Al}-X)/\text{Å}$			
	$X=\text{Al}$	O29	O4,O5,O13	Zn35	Zn8,Zn29,Zn36	O29	O4	Zn35	Zn8
25. unrelaxed	0,000	0,000	0,000	0,000	0,000	1.953	1.986	1.302	2.283
26. $\text{Al}_{i,Td}$	0.439	0.000	0.000	0.000	0.000	1.514	2.169	1.740	2.065
27. $\text{Al}_{i,Td}\text{O}_4\text{Zn}_4$	0.419	0.110	0.307	0.308	0.363	1.643	1.860	2.029	2.434

6.1.3. Optimization of the $\text{Al}_{i,Oh}$ interstitial site

The $\text{Al}_{i,Oh}$ interstitial site is located in the channels of the wurtzite structure that are visible when the structure is viewed along the crystal c -axis. Initially, the Al-atom was the placed at that point where it is

[†] These neighbors may be shortly termed 1st and 2nd coordination sphere of $\text{Al}_{i,Oh}$.

surrounded by six O-atoms at a distance of 2.283 Å in a perfectly octahedral fashion. It should be mentioned, however, that there are three shorter ionic contacts to Zn with a distance of 1.866 Å as well as three somewhat longer ones at a distance of 2.708 Å in this structure as well. All results shown in this section were calculated with 651 e^- , i.e. a formal doping of an uncharged $Al^0 (= Al_{i,oh} + 3 e^-)$, and imposed $P3m1$. The total energy per unit cell amounts to -322.840 eV (calc. 28), which is -14.637 eV (= -1412.2 kJ/mol) more stable than the (unrelaxed) $Al_{i,Td}$ interstitial site.

Optimization of $Al_{i,oh}$. Relaxation of the $Al_{i,oh}$ -site only (calc. 29) results in an energetic stabilization by -1.661 eV (= -160.3 kJ/mol) and shows a significant displacement of 0.647 Å parallel to + c that increases the short distances Zn sites mentioned above to 2.281 Å, while the distance to three of the O-sites is reduced to 1.987 Å.

Optimization of $Al_{i,oh}O_4Zn_4$. After relaxation of the Al position together with the 12 nearest neighbors mentioned above[†] (calc. 30) the structure is stabilized by -4.152 eV (= -400.6 kJ/mol) as compared to the non-relaxed structure (see Figure S7c). At this Al changes its position by 0.620 Å along + c , three of the six distances to O-atoms reduce to 1.815 Å, while the other three increase to 2.684 Å; the three shortest Zn distances mentioned above increase to 2.468 Å and the other three mentioned above reduce to 2.525 Å. A comparison of structural parameters is given in Table S8.

Table S8: Comparison of structural parameters from different optimizations of $Al_{i,oh}$ in a 3x3x2 supercell.

Calculation	$d(X-X_{unrelaxed})/\text{Å}$					$d(Al-X)/\text{Å}$			
	$X=Al$	O2,O23,O24	O3,O16,O19	Zn4,Zn32,Zn36	Zn19,Zn21,Zn35	O2	O3	Zn4	Zn19
28. unrelaxed	0,000	0,000	0,000	0,000	0,000	2.283	2.283	2.708	1,986
29.(651 e^-)	0.647	0.000	0.000	0.000	0.000	1.987	2.705	2.286	2.281
30.(651 e^-)	0.620	0.182	0.034	0.224	0.254	1.815	2.684	2.525	2.468

6.1.4. Optimization of the $[Al_2V_{Zn}]$ defect site

The hypothetical $[Al_2V_{Zn}]$ defect may occur three different configurations (see Figure S5), because the ligands of O in undoped ZnO form an imperfect tetrahedron with C_{3v} symmetry (the atomic distance to the ligand aligned along the crystal c -axis is shorter).

[†] These neighbors may be shortly termed 1st and 2nd coordination sphere of $Al_{i,oh}$.

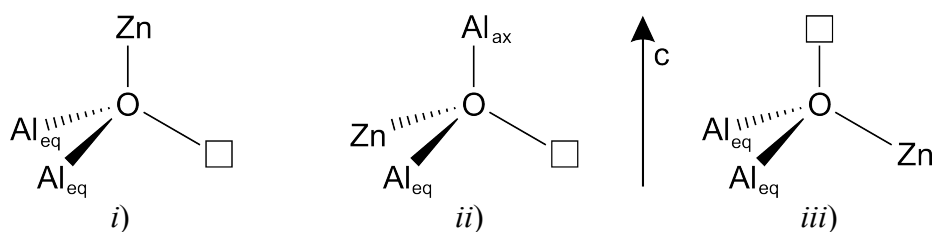


Figure S6: Three possible configurations of the (unrelaxed) $[Al_2V_{zn}]$ defect. The empty squares denote a void. Indices ax (for axial) and eq (equatorial) refer to the orientation relative to the c-axis. Configuration *ii*) can be realized in two enantiomorphs, which possess the same ^{27}Al NMR properties, however.

All three possibilities were subject to a partial structure optimization (in a $3 \times 3 \times 2$ supercell) including the central oxygen, the Al-sites and the O-sites in the first coordination sphere around Al and the void. The optimized structures are shown in Figure S7(d-e), respectively. All results shown in this section were calculated with $618e^-$, i.e. a formal doping of two uncharged Al^0 , or $Al_{zn} \cdot + 1e^-$. For the unrelaxed $[Al_2V_{zn}]$ *i*) defect the total energy per unit cell amounts to -332.143 eV (calc. 40). Upon optimization the structure stabilizes by -2.864 eV ($=-276.3$ kJ/mol). The relaxed $[Al_2V_{zn}]$ *i*) defect is the most stable one, the relaxed $[Al_2V_{zn}]$ defects *ii*) and *iii*) are less stable by 0.091 eV ($=8.8$ kJ/mol) and 0.279 eV ($=26.9$ kJ/mol), respectively.

A few structural parameters of the $[Al_2V_{zn}]$ defects are summarized in Table S9. The structural relaxation can be understood qualitatively from an electrostatic viewpoint, if the crystal is thought to be composed of positively charged Al and Zn atoms and negatively charged O atoms, as well as from a bond theoretical viewpoint. The oxygen ligands around the Al move towards the Al-sites, because Al has a higher core charge (Al^{3+}) and more compact valence orbitals than Zn. The oxygen neighbors next to the void lack an attractive force in the direction of the void, hence they move away from it. The central oxygen atom of the $[Al_2V_{zn}]$ defect shown in Figure S6 experiences both effects simultaneously and shows therefor the largest relaxation displacement.

Table S9: Structural parameters of relaxed $[Al_2V_{Zn}]$ defects obtained in a $3 \times 3 \times 2$ supercell.

Calculation	$d(X-X_{unrelaxed})/\text{Å}$			$d(Al_a-X)/\text{Å}$				$d(Al_b-X)/\text{Å}$			
	O _c	Al _a	Al _b	O _d	O _e	O _f	O _g	O _d	O _e	O _f	O _g
37. $[Al_2V_{Zn}]$ i)	0.315	0.057	0.057	1.783	1.798	1.801	1.814	1.783	1.798	1.801	1.814
40. $[Al_2V_{Zn}]$ ii)	0.322	0.074	0.095	1.758	1.786	1.798	1.857	1.725	1.779	1.824	1.893
43. $[Al_2V_{Zn}]$ iii)	0.348	0.049	0.049	1.785	1.801	1.812	1.818	1.785	1.801	1.812	1.818

O_c is the central oxygen (see Fig. S6), Al_a is always equatorial. O_d, O_e, O_f, O_g are sorted according to increased distance from Al_a or Al_b, respectively.

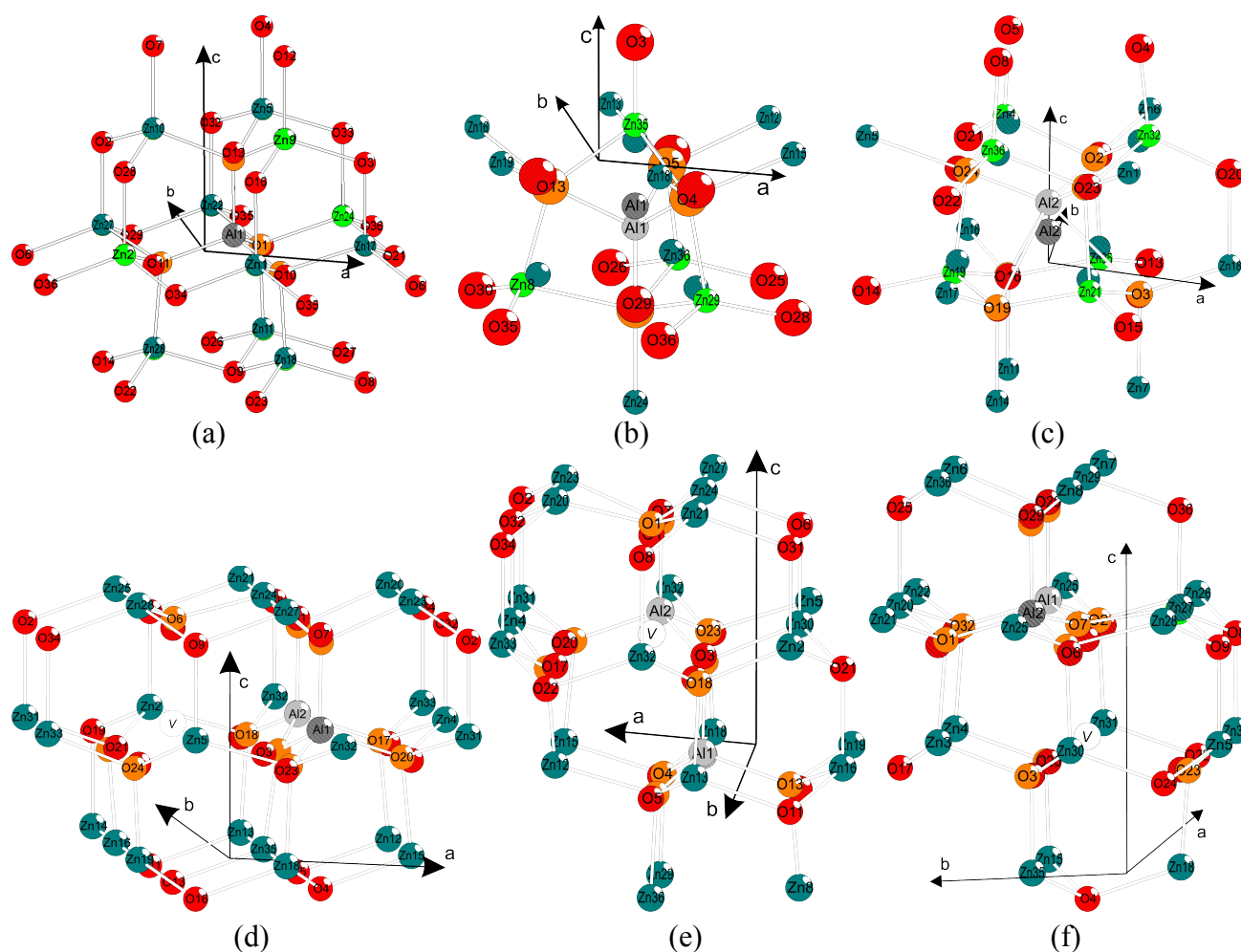


Figure S7: Comparison of non-optimized and relaxed structures of various defect sites in ZnO:Al (larger cutout than in main article). (a) Al_{Zn} , (b) Al_{iTd} , (c) Al_{iOh} , (d) $[\text{Al}_2\text{V}_{\text{Zn}}]$, config. *i*, (e) $[\text{Al}_2\text{V}_{\text{Zn}}]$, config. *ii*, (f) $[\text{Al}_2\text{V}_{\text{Zn}}]$, config. *iii*. Oxygen sites are drawn in orange if relaxed or red if unrelaxed, zinc-sites in light green (relaxed) or dark green (unrelaxed), aluminium sites in light grey (relaxed) or dark grey (unrelaxed). Non-optimized sites corresponding to optimized ones are hatched, voids are indicated by empty circles. Sites belonging to structures (a-c) are optimized up to second coordination sphere with respect to the point defects, structures (d-f) up to first sphere (see text for details).

6.2. Calculation of ^{27}Al NMR parameters by EEIM

In the present work we show that the EEIM is also suitable for the calculation of electric field gradients (EFGs) in case of crystalline and doped crystalline materials. For doped crystals a two-step procedure

(analogous to the one for σ in ref. ⁶ is proposed:

In the first step, the embedding point charges are obtained for an ideal (i.e. non-defective) crystal/quantum cluster (QC), where the usual self-consistent procedure of EEIM as described in ref. ⁷ is employed. From the ZnO crystal³ we created a roughly spherical $[\text{Zn}_{39}\text{O}_{39}]$ -QC shown in Figure S8(a) as a cutout with an embedding in 56370 point charges. Details on QC construction are given in Table S10. The optimized atomic charges for Zn and O are $\pm 1.60734 \cdot e$, respectively.

In the second step, the QC is modified to contain the (relaxed) substitutional Al_{Zn} defect close to its center, as well as an outer region in which the atomic sites of the ideal crystal are left unperturbed, i.e. the defects and the corresponding relaxations are not periodically repeated. As the charge q_{QC} of the modified QC cannot be determined exactly, it is set to a value that allows a closed shell calculation and, at the same time, is close to the sum of the expected fragment charge according to the self-consistent charges determined in the first step and the assumed defect site charge. Formal charges can be used for lowly charged defect sites, since the EEIM seems to tolerate small charge misfits of the QC.⁶ For Al_{Zn} we created two QCs, $[\text{AlZn}_{38}\text{O}_{39}]^+$ and $[\text{AlZn}_{38}\text{O}_{39}]^-$ (corresponding to Al_{Zn}^+ and Al_{Zn}^- , respectively,) which are embedded in the charge field obtained from $[\text{Zn}_{39}\text{O}_{39}]$ in the first step. $\text{Al}_{i,\text{Td}}$ was calculated analogously in a neutral $[\text{AlZn}_{38}\text{O}_{38}]$ QC, $\text{Al}_{i,\text{Oh}}$ in a $[\text{AlZn}_{42}\text{O}_{42}]$ QCs, and the $\text{Al}_2\text{V}_{\text{Zn}}$ defects in $[\text{Al}_2\text{Zn}_{46}\text{O}_{49}]$ QCs. Further details are given in Table S10. Finally, the calculation of EFG and NMR parameters is performed.

A locally dense AO basis of gaussian functions was defined by setting up three spherical regions with radial ranges r_i ($i=1,2,3$) around the substitution site. In the inner region ($r_1=[0,4[\text{\AA}$ for Al_{Zn}) the 6-311G(3df,3pd) bases^{8,9} for O and Al and the 6-31G* (all electron) atomic basis set for Zn¹⁰ were used. For selected calculations (46,47,59) we checked the basis set convergence of the EFG by using various other basis sets on the Al site, i.e. 6-31G*⁹, pcS-3¹¹ and pcS-3 with decontracted core orbitals. In the second region ($r_2=[4,5[\text{\AA}$ for Al_{Zn}) the 6-31G* basis set was used for O, and the CEP-4G set for Zn¹² with corresponding pseudo potentials for the core electrons. CEP-4G sets with pseudo potentials were used in the outer region ($r_3 \geq 5\text{\AA}$ for Al_{Zn}) for the remaining atoms. The same AO bases with slightly different radial ranges r_i were used for the other defects (see Table S10), except for $\text{Al}_{i,\text{Td}}$ where an Ahlrichs-VTZ basis¹³ was used for the nearest Zn atoms. Tight convergence criteria were chosen, corresponding to maximum deviations in density matrix elements of 10^{-8} and in the energy of 10^{-8} Hartree. Quadrature was performed on an ultra fine grid, i.e. a grid of 99 radial shells and 590

angular points per shell on each atom. For some calculations using the (decontracted) pcS-3 basis set, a number of 159 radial shells was required to reach convergence. Only restricted wave functions were allowed. The derivatives required for the computation of the ^{27}Al EFG tensors \mathbf{q} were calculated analytically using the aforementioned model/basis set combination. Absolute nuclear magnetic shielding tensors σ were calculated using the GIAO formalism.¹⁴ The derivation of a conversion equation from absolute magnetic shieldings σ (^{27}Al) to chemical shift values δ (^{27}Al) is hampered by the fact that the currently used ^{27}Al chemical shift reference is essentially hydrated Al^{3+} ions (the reference compound is a solution of $\text{Al}(\text{NO}_3)_3$ 1.1 mol kg^{-1} in D_2O)¹⁵ whose dynamical behavior makes a quantum chemical modeling difficult. Instead, we used solid $\alpha\text{-Al}_2\text{O}_3$ as a secondary reference, whose crystal structure at 300 K was published by Ishizawa *et al.*¹⁶ (ICSD 10425) and whose experimental isotropic chemical shift has been determined to $\delta_{iso}^{\text{exp}}=18.8$ ppm by Vosegaard and Jakobsen¹⁷ and to 16.0 ppm by Skibsted *et al.*¹⁸. We used the first value in the conversion equation 1 for a given sample s .

$$\delta^{\text{calc}}(s) = \sigma_{iso}^{\text{calc}}(\alpha\text{-Al}_2\text{O}_3) - \sigma^{\text{calc}}(s) - \delta_{iso}^{\text{exp}}(\alpha\text{-Al}_2\text{O}_3) \quad (1)$$

$\sigma_{iso}^{\text{calc}}(\alpha\text{-Al}_2\text{O}_3)$ is calculated with the same quantum chemical model and basis functions as $\sigma^{\text{calc}}(s)$, as far as possible, to cancel out systematic basis set errors. An EEIM procedure using $[\text{Al}_{14}\text{O}_{21}]$ -QCs in 77725 embedding charges resulted in $\sigma_{iso}^{\text{calc}}(\alpha\text{-Al}_2\text{O}_3)=578.68$ ppm for 6-31G*, 557.78 ppm for 6-311G(3df,3pd), 555.98 ppm for pcS-3 and 555.66 ppm for uncontracted pcS-3. Details are shown in Table S10. The similarity between 6-311G(3df,3pd) and (uncontracted) pcS-3 shieldings indicates that the basis expansion is sufficiently converged.

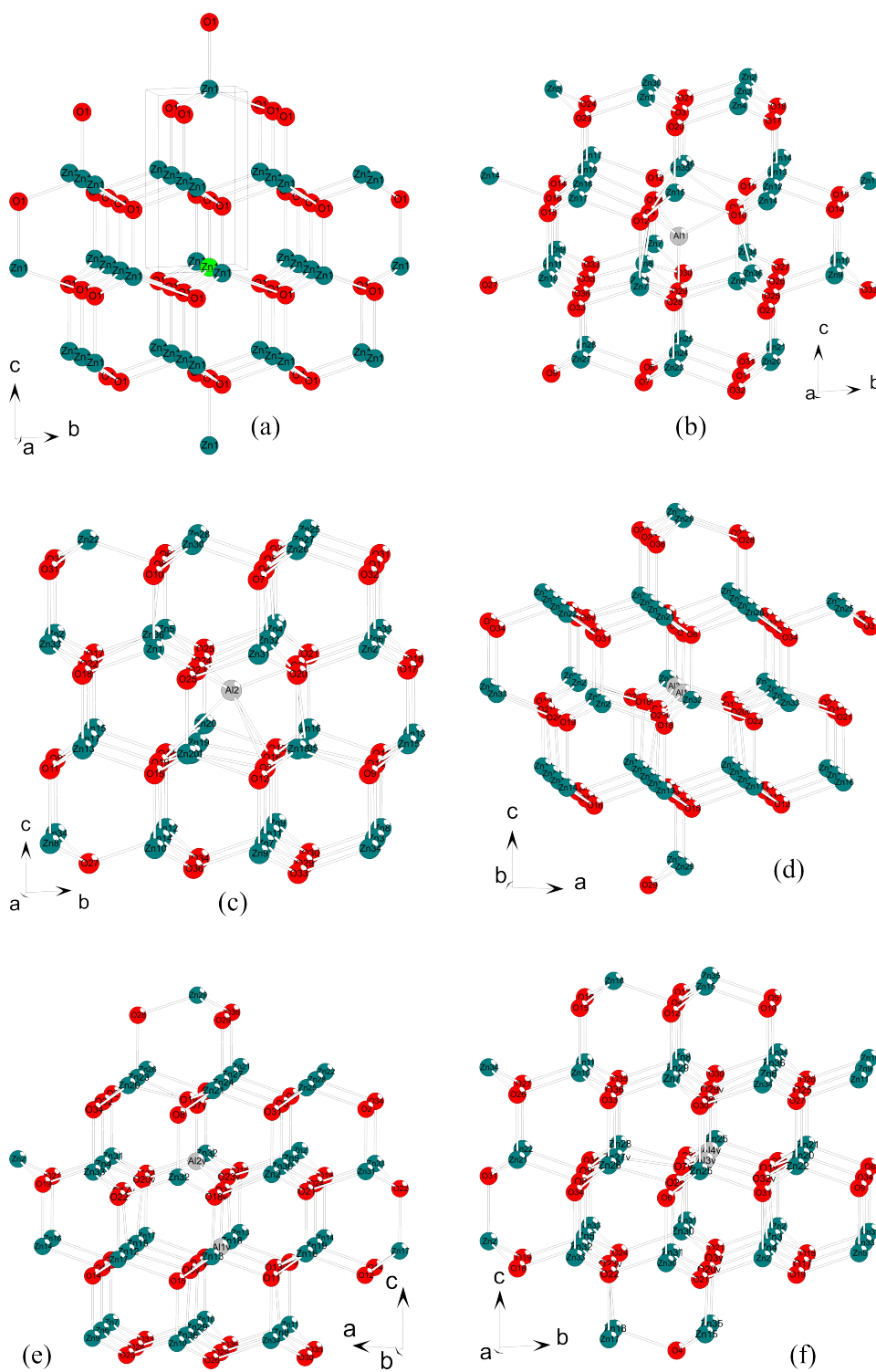


Figure S8: Quantum clusters used in EEIM calculations. (a) used for determination of embedding charges and for Al_{Zn} (defect substitutes highlighted Zn, calcs. 46-53); (b) used for $Al_{i,Td}$ (calc. 54); (c) used for $Al_{i,Oh}$ (calc. 55); (d) used for $[Al_2V_{Zn}]i$ (calc. 56); (d) for $[Al_2V_{Zn}]ii$ (calc. 57); (d) used for $[Al_2V_{Zn}]iii$ (calc. 58).

Table S10: Setup of EEIM cluster calculations at mPW1PW level for defect structures from VASP optimized structures

calc. no.	defect	struct. opt. no ^a	QC	basis	atom	range/Å ^b	N_a, N_b, N_c	$[N_1+N_2]$	N_{rep} ^c
46	Al _{Zn}	0	[AlZn ₃₈ O ₃₉] ⁻	6-311G(3df) 6-31G(d) 6-31G(d) CEP-4G CEP-4G	Al,O Zn O Zn O	$r_s < 4.0$ $r_s < 4.0$ $r_s \in [4,5[$ $r_s \geq 4.0$ $r_s \geq 5.0$	5, 5, 5	600	2000
47	Al _{Zn}	0	[AlZn ₃₈ O ₃₉] ⁺	same as in calc. 46			5, 5, 5	600	2000
48	Al _{Zn}	7	[AlZn ₃₈ O ₃₉] ⁻	same as in calc. 46			6, 6, 6	600	2300
49	Al _{Zn}	7	[AlZn ₃₈ O ₃₉] ⁺	same as in calc. 46			6, 6, 6	600	2300
50	Al _{Zn}	8	[AlZn ₃₈ O ₃₉] ⁻	same as in calc. 46			6, 6, 6	600	2300
51	Al _{Zn}	8	[AlZn ₃₈ O ₃₉] ⁺	same as in calc. 46			6, 6, 6	600	2300
52	Al _{Zn}	9	[AlZn ₃₈ O ₃₉] ⁻	same as in calc. 46			6, 6, 6	600	2300
53	Al _{Zn}	9	[AlZn ₃₈ O ₃₉] ⁺	same as in calc. 46			6, 6, 6	600	2300
54	Al _{<i>i,Td</i>}	27	[AlZn ₃₈ O ₃₈] ⁺	6-311G(3df) Ahlr.-VTZ ^d 6-31G(d) CEP-4G CEP-4G	Al,O Zn O Zn O	$r_s < 3.7$ $r_s < 3.6$ $r_s \in [3.7,4.8[$ $r_s \geq 4.0$ $r_s \geq 5.0$	6, 6, 6	600	2300
55	Al _{<i>i,Oh</i>}	30	[AlZn ₄₂ O ₄₂] ⁺	6-311G(3df) Ahlr.-VTZ ^d 6-31G(d) CEP-4G	Al,O Zn O,Zn O,Zn	$r_s < 3.7$ $r_s < 3.7$ $r_s \in [3.7,4.3[$ $r_s \geq 4.3$	6, 6, 6	600	2300
56	[Al ₂ V _{Zn}] <i>i</i>	39	[Al ₂ Zn ₄₆ O ₄₉] ⁰	6-311G(3df) 6-31G(d) 6-31G(d) CEP-4G	Al,O Zn O O,Zn	$r_s < 2.5$ $r_s < 4.0$ $r_s \in [2.5,4.0[$ $r_s \geq 4.0$	6, 6, 6	600	2300
57	[Al ₂ V _{Zn}] <i>ii</i>	42	[Al ₂ Zn ₄₆ O ₄₉] ⁰	same as in	calc.	56	6, 6, 6	600	2300
58	[Al ₂ V _{Zn}] <i>iii</i>	45	[Al ₂ Zn ₄₆ O ₄₉] ⁰	same as in	calc.	56	6, 6, 6	600	2300
59	Al ₂ O ₃ ^e	--	[Al ₁₄ O ₂₁] ⁰	6-311G(3df) 6-31G(d)	Al,O Al,O	$r_s < 2.5$ $r_s \geq 2.5$	9, 9, 4	500	2000

^a Number of VASP calculation, in which the defect structure was optimized (see Table S1).

^b is the shortest distance to one of the Al atoms in the cluster.

^c These quantities define the embedding charges. N_a, N_b, N_c define the replication of the unit cell, N_1 and N_2 the number of atoms in EEIM zones 1 and 2, respectively, and N_{rep} the number of random checkpoints for the electrostatic potential. For details, ref. ⁷

^d Ahlrichs VTZ set¹³

^e no defect, but reference compound for chemical shift calculation.

7. References

1. Y. Ishii, R. Tycko, *J. Magn. Reson.*, 2000, **142**, 199–204.
2. P. E. Blöchl, O. Jepsen, O. K. Andersen, *Phys. Rev. B*, 1994, **49**, 16223–16233.
3. R. B. Heller, J. McGannon, A. H. Weber, *J. Appl. Phys.*, 1950, **21**, 1283–1284.
4. H. J. Monkhorst, J. D. Pack, *Phys. Rev. B*, 1976, **13**, 5188–5192.
5. H. A. Jahn, E. Teller, *Proc. R. Soc. London, Ser. A*, 1937, **161**, 220–235.
6. Y. S. Avadhut, J. Weber, E. Hammarberg, C. Feldmann, I. Schellenberg, R. Pöttgen, J. Schmedt auf der Günne, *Chem. Mater.*, 2011, **23**, 1526–1538.
7. J. Weber, J. Schmedt auf der Günne, *Phys. Chem. Chem. Phys.*, 2010, **12**, 583–603.
8. A. D. McLean, G. S. Chandler, *J. Chem. Phys.*, 1980, **72**, 5639–5648.
9. M. M. Francl, W. J. Pietro, W. J. Hehre, J. S. Binkley, M. S. Gordon, D. J. DeFrees, J. A. Pople, *J. Chem. Phys.*, 1982, **77**, 3654–3665.
10. V. Rassolov, J. A. Pople, M. Ratner, T. L. Windus, *J. Chem. Phys.*, 1998, **109**, 1223–1129.
11. F. Jensen, *J. Chem. Theory Comput.*, 2008, **4**, 719–727.
12. W. J. Stevens, M. Krauss, H. Basch, P. G. Jasien, *Can. J. Chem.*, 1992, **70**, 612.
13. A. Schäfer, H. Horn, R. Ahlrichs, *J. Chem. Phys.*, 1992, **97**, 2571–2577.
14. K. Wolinski, J. F. Hinton, P. Pulay, *J. Am. Chem. Soc.*, 1990, **112**, 8251–8265.
15. M. J. Alam, D. C. Cameron, *J. Vac. Sci. Technol. A*, 2001, **19**, 1642.
16. N. Ishizawa, T. Miyata, I. Minato, F. Marumo, S. Iwai, *Acta Cryst. B*, 1980, **36**, 228–230.
17. T. Vosegaard, H. J. Jakobsen, *J. Magn. Reson.*, 1997, **128**, 135–137.
18. J. Skibsted, N. C. Nielsen, H. Bildsøe, H. J. Jakobsen, *J. Magn. Reson.*, 1991, **95**, 88–117.